International Journal of Emerging Technology and Advanced Engineering
Website: www.ijetae.com (ISSN 2250-2459, ISO 9001:2008 Certified Journal, Volume 5, Issue 11, November 2015)

Life Prediction of Low Cycle Fatigue Behavior in Rotating Cantilever Beam of Al- alloy AA 6063-T6 at Room Temperature

Mazin Mahmood Yahya[1], Nilanjan Mallik[2], I Chakrabarty[3]

[1]*Research Scholar,* [2]*Senior Assistant Professor, Mechanical Engineering Dept., IIT (BHU), Varanasi -221005, India*
[3]*Associate Professor, Metallurgical Engineering Dept., IIT (BHU), Varanasi-221005, India*

***Abstract*— In this paper low cycle fatigue analysis of AA-6063 alloy is presented theoretically and experimentally for circular cross section subjected to monotonic and cyclic elastic–plastic pure bending. The rotating bending approach is adopted for determination of low-cycle fatigue parameters. The stress ratio R = -1 is induced on the circular cross-section cantilever specimen loaded with a pure bending moment, and exposed to the rotation with respect of its longitudinal axis. The cyclic strain–stress response and strain life fatigue curves are plotted. The cyclic strain hardening exponent, cyclic strength coefficient, fatigue strength exponent and fatigue ductility exponent were found to be almost constant, being 0.06153, 219.29 MPa, -0.06153 and -1.1 respectively. It is found that theoretical values of cyclic strain hardening exponent (n') and cyclic strength coefficient (K') are in good agreement to that obtained experimentally. A log-log strain-life curve is presented and all fatigue parameters are predicted. Fatigued samples were examined using scanning electron microscopy (SEM) and optical microscopy in order to understand the failure mechanism.**

***Keywords*— Low cycle Fatigue (LCF), rotating bending cantilever beam, cyclic stress – strain response, strain life curve, low cycle fatigue parameters.**

I. INTRODUCTION

Because of their technological importance and their exceptional increase in strength obtained by precipitation hardening Al–Mg–Si (6xxx) alloys have been studied extensively. The 6*xxx*-group contains magnesium and silicon as major additional elements. These multiphase alloys belong to the group of commercial aluminum alloys, in which relative volume; chemical composition and morphology of structural constituents exert significant influence on their useful properties.

The exceptional increase in strength obtained by precipitation hardening Al–Mg–Si (6xxx) alloys, the Al–Mg–Si alloys are mostly used in extruded Al products, as well as for construction and automotive purposes, the ease with which these alloys can be shaped, their low density, their very good corrosion-and surface-properties and good weldability are factors that together with a low price make them commercially very attractive. Fatigue is the progressive, localized, and permanent structural change that occurs in a material subjected to repeated or fluctuating strains at nominal stresses that have maximum values less than (and often much less than) the static yield strength of the material. Fatigue damage is caused by the simultaneous action of cyclic stress, tensile stress, and plastic strain [1]. When the load levels are low, stresses and strains are linearly related, at high load levels in the low cycle fatigue (LCF) regime the cyclic stress-strain response and the material behavior are best modeled under strain-controlled conditions, Bannantine J.A. et. al [2]. Basquin [3] observed that for steel and copper materials the stress-life data could be linearized on log–log scale. The strain-based approach for fatigue problems is widely used at present, especially in the low-cycle fatigue (LCF) loading of machine parts and structures [4-5]. Since fatigue damage is assessed directly in terms of local strain, this approach is also called the ‘‘local strain approach”. Salerno et al. [6] applied classical criteria for the LCF lifetime estimation of AA7175-T1 aluminum alloy to consider the mean strain effect. Minichmayr et al. [7] carried out Low Cycle Fatigue LCF lifetime assessment of aluminum alloys using the damage rate model of Sehitoglu. Energy-based prediction of LCF lifetime of steel bars was done by Abd alla et al. [8] under various strain ratios.

International Journal of Emerging Technology and Advanced Engineering
Website: www.ijetae.com (ISSN 2250-2459, ISO 9001:2008 Certified Journal, Volume 5, Issue 11, November 2015)

N Eswara Prasad et al. [9] have taken aluminium–lithium alloys and studied the structure and mechanical properties with a view to indicate the directions that have been and can be pursued to overcome property limitations.

The present paper deals with low cycle fatigue analysis of AA6063 aluminium alloy at room temperature. The study is performed both theoretically and experimentally. Circular cross-section rotating bending specimen is chosen for the experimental study. Fatigue parameters and transition fatigue life were predicted from the study and compared with that obtained theoretically.

II. Methodology

A. Experiments

1. Chemical Composition Analysis

Chemical composition test are performed using "Thermo Scientific ARL Optim: X-Ray Analyzer 166" with supply voltage 230V-1.5 KV to understand the chemical composition of the specimen. Chemical composition is also studied through EDAX analysis. The quantitative analysis by EDAX is performed with a relatively high voltage of 10 KV to improve the contrast between metallic and matrix phases. Microstructural features and failure mechanisms are studied through scanning electron microscopy (SEM). The SEM-EDAX system used is FEG Quanta -200.

2. Tensile test

Before fatigue test, the monotonic tensile test is performed with cylindrical Hounsfield tensile specimen with gauge length 15.4 mm and gauge diameter 4.5 mm as shown in Fig. 1, at a nominal strain rate of $1.2 * 10^{-4}$ s^{-1} using Instron 4206 machine (Fig. 2) having loading capacity of 100KN. The test is performed with the methods specified by ASTM Standards E8 and E606, respectively.

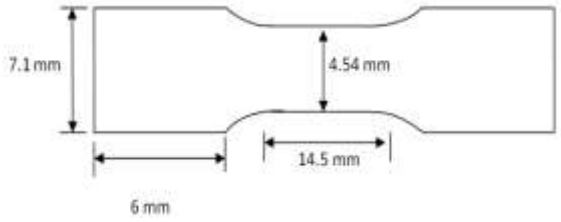

Fig. 1 Tensile Test Specimen

Fig. 2 Tensile Testing Machine

3. Torsion test

Torsion test is also performed with the sample as shown in Fig. 3 using Avery, Birmingham, England make torsion testing machine having 60000 kg-cm capacity.

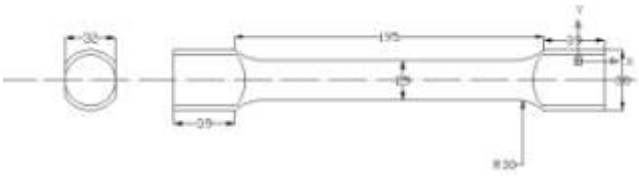

Fig. 3 Torsion Test Specimen

4. Fatigue test

Figure 4 shows the geometry of the cantilever fatigue specimen with gage length 106 mm and gage diameter 8 mm. The test is done using WP 140 Fatigue Testing Apparatus of Gunt, Hamburg, Germany as shown in Fig. 5.

International Journal of Emerging Technology and Advanced Engineering
Website: www.ijetae.com (ISSN 2250-2459, ISO 9001:2008 Certified Journal, Volume 5, Issue 11, November 2015)

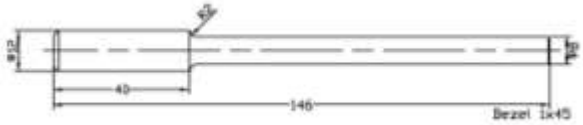

Fig. 4 Cantilever Fatigue Test Specimen

Fig. 5 Cantilever Fatigue Testing Machine

5. X-RD test

Grain size of tested samples is calculated using X-ray diffraction (XRD) method.

6. Optical micrograph test

Optical micrography is studied for fatigue test samples using metallux-3 optical microscope of Carl Zeiss Micro Imaging, Gmb H 37081, Germany. The samples are prepared by etching with a solution containing HNO_3, HF and water in proportion of 5%, 10% and 85% respectively, by volume.

7. Hardness test

Micro hardness test is carried out to evaluate the strength and ductility of the Al 6063 alloy subjected to the different applied load. Vickers micro hardness (HV) is measured on the plane surface with different loads. Prior to each hardness measurement, the surfaces of the specimen is polished mechanically using emery paper and alumina liquid to remove the surface reactions. An average of at least three readings on the surface of the specimen is taken to obtain a micro hardness value.

Vickers macro hardness (HV) was done using model MECH C.S/VM50 having mechatronic control system.

B. Theoretical Analysis

The theoretical investigation of low cycle fatigue (LCF) is performed using the method elaborated by Fatemi et al. [10] and Eleiche et al. [11].

According to Basquin, the stress-life data can be linearized on log-log scale as

$$\frac{\Delta\varepsilon_e}{2} = \frac{\sigma_f'}{E}(2N_f)^b \quad (1)$$

Coffin and Manson found that the plastic strain-life data could also be linearized on log–log scale as

$$\frac{\Delta\varepsilon_p}{2} = \varepsilon_f'(2N_f)^c \quad (2)$$

The total strain amplitude can then be considered as the summation of elastic and plastic amplitudes and the resulting strain-life curve can be expressed as:

$$\varepsilon_a = \frac{\Delta\varepsilon_e}{2} + \frac{\Delta\varepsilon_p}{2} = \frac{\sigma_f'}{E}(2N_f)^b + \quad (3)$$

The life at which elastic and plastic components of strain are equal is called the transition fatigue life (2Nt). For lives shorter than 2Nt the deformation is mainly plastic, whereas for lives longer than 2Nt the deformation is mainly elastic.

The cyclic strength coefficient, K′, and the cyclic strain hardening exponent, n′ can be estimated from the low-cycle fatigue parameters as follows [12]:

$$K' = \frac{\sigma_f'}{(\varepsilon_f')^{\frac{b}{c}}} \quad (4)$$

$$n' = \frac{b}{c} \quad (5)$$

III. Results And Discussion

Chemical composition results for as received AA6063 alloy at room temperature by chemical analysis method and EDAX method are shown in Table 1. Chemical composition analysis by two methods provide good agreement.

International Journal of Emerging Technology and Advanced Engineering
Website: www.ijetae.com (ISSN 2250-2459, ISO 9001:2008 Certified Journal, Volume 5, Issue 11, November 2015)

TABLE 1
CHEMICAL COMPOSITION OF AS RECEIVED AA 6063-T6 ALLOY AT ROOM TEMPERATURE

Element Weight%	Chemical Analysis	EDAX Analysis
Al (Balance)	99.17	88.60
Si	0.612	1.38
Mg	0.0798	0.82
Fe	0.0280	0.98
Cu	0.0374	0.64
Zn	0.0019	0.63
Mn	0.0132	0.51
Ti	0.0024	0.49
Cl	--	0.36
Ga	0.0197	--
S	0.0193	--
Ho	0.0070	--
Pb	0.0019	--
O	--	5.60
Error	0.83	0.26

Table 2 shows the results of the tensile test. The log-log plot of the completely reversed stabilized cyclic true plastic stress versus true plastic strain can be approximated by a straight line to obtain the values of strain hardening exponent (*n)* and strength coefficient (K).

TABLE 2
TENSILE PROPERTIES OF AS RECEIVED AA 6063-T6 ALLOY AT ROOM TEMPERATURE

Parameter	Symbol	Value
Yield stress	σ_{YD}	169.67 MPa
Max. tensile stress	$\sigma_{Max.}$	214.8 MPa
Fracture strength	σ_f	54.2 MPa
Yield strain	ε_{YD}	0.002457
Young's modulus	E	68 GPa
% Strain at failure	ε_f	0.242
Toughness	K_c	41.417 m^3/J
Strength coefficient	K	776.2 MPa
Strain hardening exponent	n	0.25

Table 3 shows torsion test parameters which are calculated from torque and angle of twist curve obtained from torsion test.

TABLE 3
TORSION TEST DATA FOR AS RECEIVED AA 6063-T6 ALLOY AT ROOM TEMPERATURE

Parameters	symbol	Value
Max. shear strain	γ_{max}	6.4 Deg.
Max. angle of twist	θ_{max}	100
Shear modulus	G	32.373 GPa
Toughness	K_t	914 J/m^3
Max. shear stress	τ_{max}	209.03 MPa
Torque	T_{max}	641.3 Nm

Table 4 elaborates micro hardness test results. The Vickers macro hardness values are given in Table 5. The crystal structure in the sample is investigated through XRD analysis. The intensities and the angular position of the Bragg peaks in the diffraction pattern shown are in Fig. 6. The XRD spectra of the sample clearly show the major 2θ peaks of Al. The diameters of the crystallize size and intensity of Bragg peaks at different 2θ angles are obtained from experimental results without loading as shown in Fig. 6.

TABLE 4
VICKERS MICRO HARDNESS VALUES FOR AS RECEIVED AA 6063-T6 ALLOY AT DIFFERENT LOAD

Load applied (KG)	Micro HV
0.05	99.7875
0.09	100.575
0.19	100.725

TABLE 5
VICKERS MACRO HARDNESS VALUES FOR AS RECEIVED AA 6063-T6 ALLOY AT DIFFERENT LOAD

Load applied (KG)	Macro HV
1	46.076
2	43.07
3	44.36
5	19.2
10	13.3

International Journal of Emerging Technology and Advanced Engineering
Website: www.ijetae.com (ISSN 2250-2459, ISO 9001:2008 Certified Journal, Volume 5, Issue 11, November 2015)

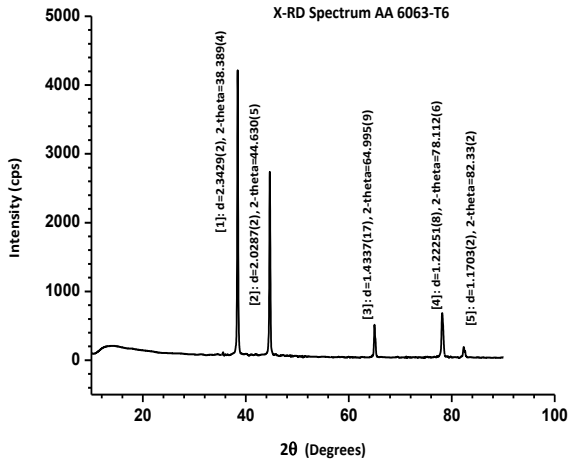

Fig. 6 X-RD Pattern for as received AA6063-T6 alloy at room temperature

The results obtained from XRD analysis are compared with the results given in JCPDF Table 6 (Joint Committee for Powder Diffraction Standards) File No.851327 for aluminium Cubic system. The micro structural information is predicted from broadening of the Bragg peaks. The total broadening is due to instrumental broadening and broadening due to average domain size and the lattice micro strains. The X-RD test was also done for the samples at different loads e. g. in elastic zone at 4.5Kg, at yield point at 6.9Kg and in plastic zone at 7.839Kg and at 8.55Kg. Different crystallite sizes are obtained at different loads as illustrated in Table 7. It is also observed from Fig. 8 that the crystallite size increases with increase in load.

TABLE 6
CRYSTALLITE SIZE AND INTENSITY DATA FOR AS RECEIVED AA 6063-T6 ALLOY AT ROOM TEMPERATURE

Sl. NO.	H k l Miller indices of the Bragg reflections	d(A)		Intensity	
		JCPDF	A6063-T6 Expt. XRD	JCPDF	A6063-T6 Expt. XRD
1	1 1 1	2.3379	2.34286	999	716.41
2	2 0 0	2.0247	2.02868	455	509.44
3	2 2 0	1.4316	1.43371	233	111.73
4	3 1 1	1.2209	1.22251	228	211.58
5	2 2 2	1.689	1.17027	63	50.27

TABLE 7
CRYSTALLITE SIZE AND DIAMETER FOR AS RECEIVED AA 6063-T6 ALLOY AT DIFFERENT LOAD

Diameter at fracture	Load	Crystallite size (nm)
Non (It is square sample)	Without load before test (as received)	91.834
6.2 mm	4.5 kg (44.145N)	128.24
7 mm	6.9 kg (67.68N)	166.84
6.6 mm	7.38 kg (72.5N)	122.922
6.94 mm	8.55 kg (83.8N)	152.989

TABLE 8
CYCLIC DATA FOR CANTILEVER BEAM FATIGUE TEST OF AS RECEIVED AA-T6 ALLOY AT ROOM TEMPERATURE

Force (N)	True Stress (MPa)	Number of cycles to failure (N_f)	Total strain amplitude	Elastic strain amplitude	Plastic strain amplitude
19.8	41.41	141300	6.09E-4	6.09E-4	0
24.0	49.67	166560	7.3E-4	7.3E-4	0
28.4	57.94	43560	8.52E-4	8.52E-4	0
32.7	65.65	63300	9.65E-4	9.65E-4	0
37.1	73.07	60150	0.00107	0.00107	0
39.4	76.68	15990	0.00113	0.00113	0
41.6	80.17	9750	0.00118	0.00118	0
46.1	86.66	6690	0.00127	0.00127	0
58.8	102.9	3000	0.00151	0.00151	0
67.9	112.8	907	0.00166	0.00166	0.000052
72.4	117.3	1708	0.00172	0.00172	0.00051
76.4	121.0	876	0.00178	0.00178	0.00081
83.9	177.0	444	0.0053	0.0026	0.00271
86.6	182.8	380	0.00575	0.00269	0.00307
94.5	199.4	350	0.00727	0.00293	0.00435
110	233.6	280	0.01158	0.00343	0.00818
120	253.6	200	0.01502	0.00372	0.0113
130	275.5	176	0.01974	0.00404	0.01576
140	295.4	133	0.02502	0.00434	0.02077

The cyclic data have been collected and given in Table 8 and transition fatigue life were determined from intersection of the $\frac{\Delta\varepsilon_e}{2}$ vs 2Nf and $\frac{\Delta\varepsilon_p}{2}$ vs *2Nf* plots as illustrated in Fig. 7.

International Journal of Emerging Technology and Advanced Engineering
Website: www.ijetae.com (ISSN 2250-2459, ISO 9001:2008 Certified Journal, Volume 5, Issue 11, November 2015)

In this figure, the life at which the two lines for regions I (elastic) and II (plastic) of the model intersect is called the separation fatigue life ($2N_t$), with the true stress amplitude at that life denoted by $\frac{\Delta\sigma_s}{2}$. Experimental fatigue parameters $\acute{n}$ and $\acute{k}$ of the aluminum alloy are found out from the strain –life curve (log–log S–N) shown in Fig. 7. The comparison of values of n' and K' are shown in Table 9. The experimental LCF parameters viz. fatigue strength coefficient (σ_f') fatigue strength exponent (b), fatigue ductility coefficient (ε_f') and fatigue ductility exponent (c) are also obtained from Fig. 7 and are shown in Table 10.

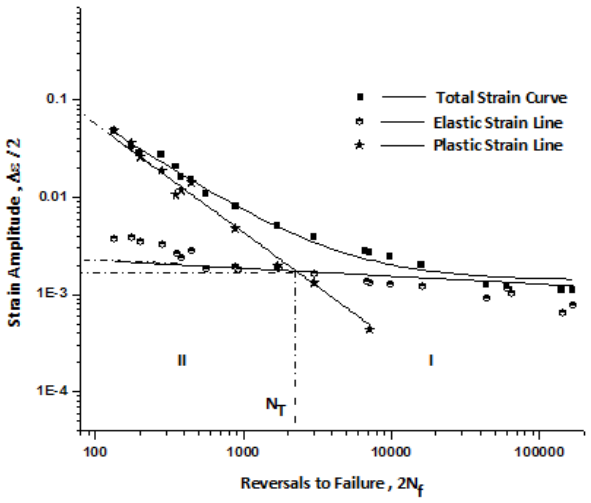

Fig. 7: Strain life Curve for as received AA6063-T6 alloy at Room Temperature

TABLE 9
n' AND K' VALUE EXPERIMENTALLY AND THEORETICALLY

parameters	experimental	theoretical
n'	0.06153	0.05
K'	219.29	310

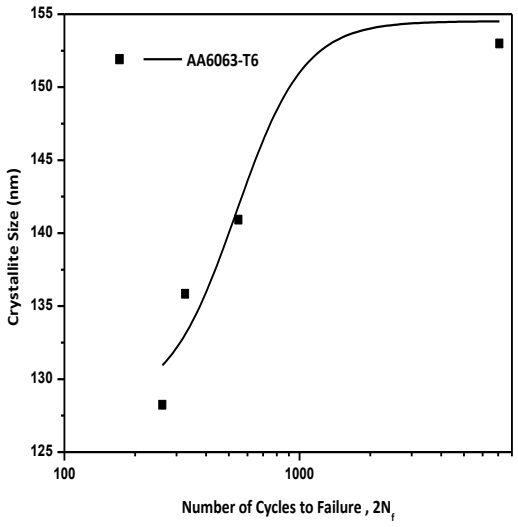

Fig. 8 Crystallite Size with the Number of Cycles to Failure

TABLE 10
STRAIN-CONTROLLED FATIGUE PROPERTIES OF AS RECEIVED AA 6063-T6 ALUMINUM ALLOY

Alloy	Cyclic plastic strain (Fatigue Ductility coefficient) ε_f'	Cyclic elastic strain σ_f'/E	Fatigue Strength Coefficient σ_f' (MPa)	fatigue strength exponent b	fatigue ductility exponent c	cyclic strain hardening exponent n´	cyclic strength coefficient K´ (MPa)	transition fatigue life N_T (cycles)
6063-T6	0.0687	0.002735	185.98	-0.08	-1.1	0.06153	219.29	2150

International Journal of Emerging Technology and Advanced Engineering
Website: www.ijetae.com (ISSN 2250-2459, ISO 9001:2008 Certified Journal, Volume 5, Issue 11, November 2015)

Figure 8 illustrates that crystallite size increases with increase in number of cycles of failure. It is also observed in Fig. 9 that as the number of cycles of failure reduced, so does the hardness value in LCF region.

To study the microstructure features Optical Micrograph pictures were taken with different magnification before test as shown in Fig. 10 and after test as shown in Fig. 11.

Figures 12 and 13 shows scanning electron micrograph pictures of the samples before and after test at different magnifications at two different location viz. at yield point and at plastic zone, respectively. All fracture surfaces had a dimple morphology at 47x magnification with an yield point as illustrated in Fig. 12(a). This indicates ductile fracture mode. Most of these dimples resulted from fracture or decohesion of Si & Mg particles.

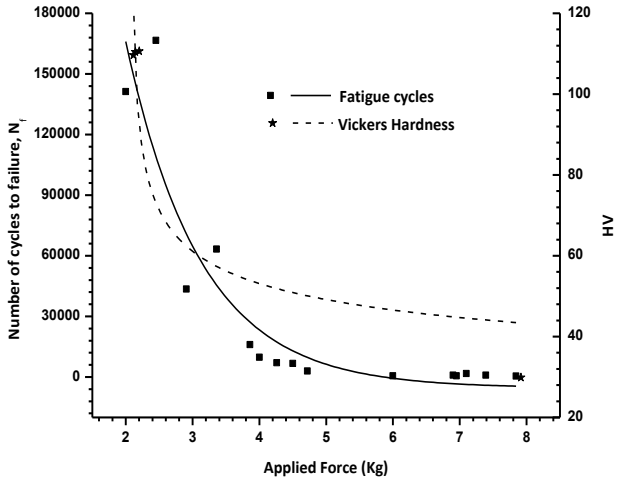

Fig. 9 Variation of Number of Cycles and Vickers Hardness with Applied Force for AA6063 as received

(a) (b)

Fig. 10 Optical Micrograph for AA6063 Samples as received before the test at:
(a) 50x magnification, (b) 100x magnification

The second population consisted of very small dimples located in the space between the reinforcement particles associated with the intermetallic particles.

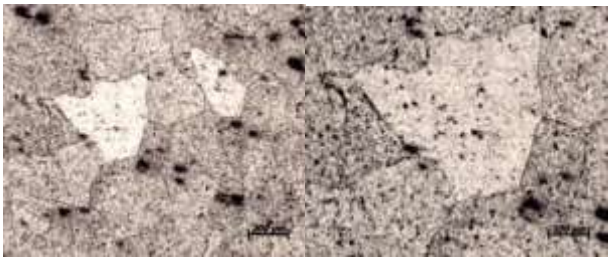

(a) (b)

Fig. 11: Optical Micrograph for AA6063 Samples as received after the test at:
(a) 50x magnification , (b) 100x magnification

A cross-sectional (over view) of this fatigue failure shows that the piece is domed with the smallest radius near the outer edge. This small radius testifies to a high stress concentration. Also of interest is the shape of the overload zone. The fact that it is elongated indicates some plane bending loads were present. We have seen more than one point of origin where the crack actually started, and that indicates the presence of multiple origins which may be the result of either high stress or high stress concentrations. From edge more than one point of origin can be seen of crack as illustrates in Fig. 12(b) at 160x magnification, which indicates the result of either high stress or high stress concentrations.

A view in Fig. 12 shows two ratchet marks separating the three failure origins. It can be noted that the origins are not on the same plane and that the ratchet marks are in effect boundaries between the fracture planes. In fact, there is yet another origin on the other side of the failure face.

There were a few observations of pull out of particles from the Al-matrix, which indicates quite a good interfacial bonding. From the figure the plateau etching can be observed which shows the fracture and microstructure features.

In Fig. 12, at center i.e. crack propagation region for 600x magnification and 164.9 MPa yield point, shows a this picture that look like a river on physical map, which show the direction of progression of the fatigue crack. In same time at high magnification we can see the progression Marks (beach marks) , and these marks will tell exactly how the crack face has progressed across the test piece and are only present in fractures .

International Journal of Emerging Technology and Advanced Engineering
Website: www.ijetae.com (ISSN 2250-2459, ISO 9001:2008 Certified Journal, Volume 5, Issue 11, November 2015)

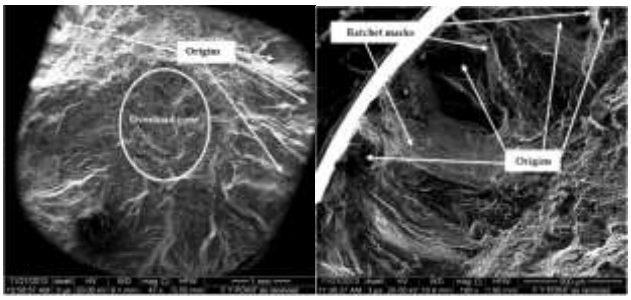

(a) (b)

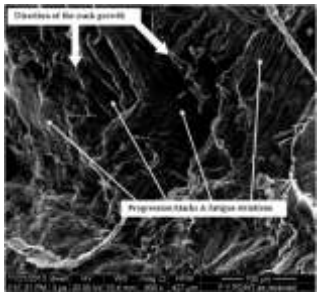

(c)

Fig. 12: SEM Pictures after the LCF test at the Yield point at: (a) 47x magnification, (b)160x magnification, (c) 600x magnification

The crack face has progressed across the test piece and is only present in fractures. Ductile striations with large, regular size and spacing can be observed from Fig. 13 .

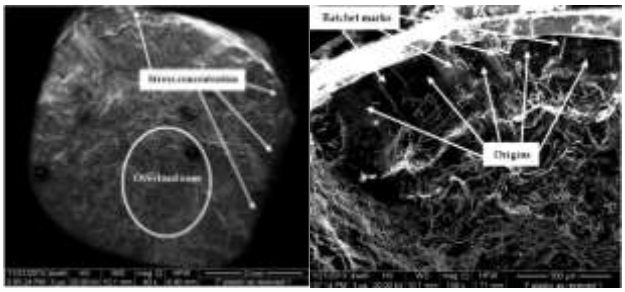

(a) (b)

Fig. 13: SEM Pictures after the LCF test at the plastic zone at: (a)40x magnification ,(b) 150x magnification

Most of these dimples resulted from fracture or decohesion of Si & Mg particles. From edge (initiation crack) plastic zone 150x as shown in Fig. 13 (b) , more than one point of origin can be seen where the crack actually started, and that indicates the presence of multiple origins which may be the result of either high stress or high stress concentrations.

Again Fig. 13(b) shows more than one point of origin where the crack actually started, and that may be the result of either high stress or high stress concentrations. In same time at high magnification we can see the ratchet mark between each two origin points, and we can see the progression marks or beach marks, and these marks tell us exactly how the crack face has progressed across the piece test and are only present in fractures there have been substantial variations in the component stress as the crack grew across the piece.

Appearance of regular fatigue striations due to regular loading, still one striation per cycle. The picture shows us look like a river on physical map so, show the direction of progression of the fatigue crack. And show up most frequently in the relatively fast-growing sections of the fatigue zone, and, other than indicating the direction of the crack growth.

In same time at high magnification we can see the Progression Marks (beach marks) , and these marks tell us exactly how the crack face has progressed across the piece test and are only present in fractures there have been substantial variations in the component stress as the crack grew across the piece . Appearance of regular fatigue striations due to regular loading, still one striation per cycle, and it is called ductile striations with large, regular size and spacing.

IV. Conclusion

In the present paper, low cycle fatigue behavior of as received Al 6063-T6 at room temperature is investigated using rotating cantilever bending test. The fatigue parameters are calculated. There parameters are also obtained through an analytical approach and found to match with that obtained experimentally, additionally tensile parameters also obtained from tensile test. Microstructural observation are also done using both optical microscopy and scanning electron microscopy. Effect of variation of hardness on fatigue life is presented. Crystallite size is calculated from X-RD test without loading and with different loading.

The following conclusions are drawn from the investigation:

1. LCF analysis of AA6063-T6 Alloy was performed experimentally and result verified with that obtained theoretically.
2. A good agreement it observed between experimental and theoretical values of LCF parameters.
3. SEM analysis shows that the failure occurred due to LCF loading.
4. It is also observed as the number of cycles of failure reduced, so does the hardness value in LCF region.

REFERENCES

[1] T.A.I.H., 1996. volume 19, Fatigue and Fracture ASM Handbook .

[2] Bannantine, J.A., J.J. Comer, and J.L. Handrock, Vol. 90. 1990, Fundamentals of metal fatigue analysis: Prentice Hall Englewood Cliffs, NJ.

[3] OH, B., The exponential law of endurance tests. Am Soc Testing Mater Proc 1910. 10: p. 625–30.

[4] Knez, M., et al., A rotating bending approach for determination of low-cycle fatigue parameters. International Journal of Fatigue, 2010. 32 p. 1724-1730.

[5] Radaj D, S.C., Fatigue assessment of welded joints by local approaches. Cambridge: Abington Publishing, 1998.

[6] Salerno, G., R. Magnabosco, and C.d. Moura Neto, Mean strain influence in low cycle fatigue behavior of AA7175-T1 aluminum alloy. International Journal of Fatigue, 2007. 29(5): p. 829-835.

[7] Minichmayr, R., et al., Thermo-mechanical fatigue life assessment of aluminium components using the damage rate model of Sehitoglu. International Journal of Fatigue, 2008. 30(2): p. 298-304.

[8] Abdalla, J., et al., Energy-based prediction of low-cycle fatigue life of BS 460B and BS B500B steel bars. Materials & Design, 2009. 30(10): p. 4405-4413.

[9] Eswara Prasad, N., A. Gokhale, and P. Rama Rao. Mechanical behaviour of aluminium-lithium alloys. in Sadhana (Academy Proceedings in Engineering Sciences). 2003. Indian Academy of Sciences.

[10] A.Fatemi, A.P., A.K. Khosrovaneh, D. Tanner, Application of bi-linear log–log S–N model to strain-controlled fatigue data of aluminum alloys and its effect on life predictions. International Journal of Fatigue 2005. 27: p. 1040–1050.

[11] Eleiche, A.M., M.M. Megahed, and N.M. Abd-Allah, Low-cycle fatigue in rotating cantilever under bending.III: Experimental investigations on notched specimens. International Journal of Fatigue, 2006. 28: p. 271-280.

[12] Stephens, R.I. Fuchs, and H. Otten, 2001Metal fatigue in engineering: Wiley New York.